Experimental study of concrete filled cold-formed steel tubular stub columns

Experimental study of concrete filled cold-formed steel tubular stub columns

Aizhu ZHU[1]; Xiaowu ZHANG[1]; Hongping ZHU[1]; Jihua ZHU[2], Yong LU[3,*]

[1] School of Civil Engineering & Mechanics, Huazhong University of Science & Technology, 430074, Wuhan, China

[2] Guangdong Province Key Laboratory of Durability for Marine Civil Engineering, School of Civil Engineering, Shenzhen University, 518060, Shenzhen, China

[3] Institute for Infrastructure and Environment, School of Engineering, The University of Edinburgh, The King's Buildings, Edinburgh EH9 3JL, UK

Corresponding Author: **yong.lu@ed.ac.uk**

Abstract

An experimental programme was conducted to investigate the compressive behaviour of concrete-filled cold-formed steel tubular (CFCFST) stub columns with thicker tubes. A total of 30 CFCFST stub columns were tested. The cold-formed square hollow section (SHS) tubes included unstiffened sections and longitudinally inner-stiffened sections using different stiffening methods. Two tubular thicknesses of 6mm and 10mm were considered. The overall nominal dimension of the steel section was 200×200mm, and the length of the stub columns was 600mm. Normal concrete and self-consolidating concrete with a nominal compressive strength of 30MPa were used to fill the cold-formed SHS steel tubes. The effects of the stiffeners on the rigidity, ductility, failure mode and average sectional strength of the CFCFST specimens were examined. The measured strengths of the CFCFST specimens were also compared with the predicted capacities using methods in various codes including AISC, BS5400, EC4, and DBJ and from a finite element (FE) analysis. Results demonstrate that the inner stiffeners affect the deformability, failure mode and overall strength of the stub columns with the 6mm-thick tubes more significantly. The DBJ code method is comparatively the best in predicting the strength capacity. Using the validated FE model, an extended analysis has been conducted and this has provided further insight into the mechanical behavior of the CFCFST specimens.

Keywords: CFCFST columns; steel tubes with thick walls; stiffened sections; self-consolidating concrete; axial compression test; strength capacity

1. Introduction

Concrete-filled steel tubular (CFST) columns have been widely used in modern buildings and bridges because of their excellent structural properties such as high strength, high ductility, large energy absorption capacity, and high cost effectiveness. Square and rectangular CFST columns are increasingly used in structures for reasons of easy beam-to-column connection, high moment capacities, and aesthetic consideration. However, the general performance of square or rectangular CFST columns is not as good as their circular counterparts, and local buckling is more likely to occur in a square or rectangular tube [1]. Uy et al. [2, 3] conducted studies to investigate the local buckling and post-local buckling behaviours of the CFST columns with welded square steel sections shown in Figs.1 (a) and (b). The nominal thickness of the steel tubes used in the above study was 3mm and sectional width ranged from 120mm to 300mm. They found that the effect of local buckling on the compressive strength of the CFST columns was significant, and recommended that such effects be included in a modified rigid plastic analysis based on the methods of existing Australian and British standards [3] for cases where plate slenderness limits are large. Ge et al. [4, 5], Kitada [6], Liu et al. [7] and Tao et al. [1, 8, 9-10] conducted experimental and numerical studies on thin-walled square and rectangular CFST columns where the steel walls were stiffened to improve their structural behaviour.

Typical steel box sections are built up by welding four plane plates, and the longitudinal stiffeners are usually welded on the plates with fillet welds as shown in Figs. 1 (c) [4], (d), (e) and (f) [1,8-10]. It is generally recognized, as evidenced in the aforementioned studies, that local buckling of steel tubes can be effectively delayed when stiffeners are provided, resulting in a marked increase in the sectional strength and relatively moderate increase in the ductility. However, local buckling or cracks along the welded corners were observed by Uy et al. [3] and Ge et al. [4] for some specimens. In fact, during the Mexico Valley earthquake, two buildings at the Pino Suarez station even collapsed completely due to cracks along welded corners and plate buckling of their steel box columns [6]. As an improved design, CFST columns with round corners similar to the section shown in Fig.2 (a) was recommended [6].

A steel section with round corners can be easily obtained using the cold-formed fabrication method. Nowadays, cold-formed steel components are also used extensively in buildings as both structural and non-structural members due to their superior performance of high strength-to-weight ratio resulted from the cold-formed process [11]. More recently, some extensive investigations into the structural performance of concrete-filled cold-formed steel (CFCFST)

members have been reported. Chitawadagi et al. [12] conducted test studies on 27 cold-formed rectangular CFST columns with thickness ranged from 1.6 to 2.65mm, and found that an increase in the wall thickness helps to postpone the local buckling failure and thus enhances the ultimate axial load carrying capacity. Zhang et al. [13, 14] studied the static and dynamic structural behaviours of unstiffened and stiffened CFCFST columns with thickness of 1.25 to 1.48mm. The stiffened steel sections were built up by welding cold-formed lipped angles and channels as shown in Figs.1 (g) and (f). It was also observed that the ultimate strength increased with the number of stiffeners, and the lips anchored with concrete very well until the specimens were damaged. Moreover, columns with more stiffeners have better ductility and energy dissipation capacity. Comparing the failure modes of thin-walled CFST columns with box sections reported in literatures, no cracks at the cold-formed corners were found.

However, the above studies have mainly been concerned with thin-walled cold-formed steel with thickness no greater than 3.0 mm. Young and Ellobody [15, 16], Uy et al. [17] conducted series of experimental study on CFST columns with unstiffened cold-formed stainless steel tubes, and the maximum tubular thickness was 6mm. With the advance of the cold-forming technology, nowadays cold-formed carbon steel sections with wall thickness even greater than 20mm are being produced and applied in structures. A number of studies [18-23] have been conducted to investigate into the structural behaviour of cold-formed square hollow section (SHS) and rectangular hollow section (RHS) tubes with tubular thickness ranging from 6 mm to 16 mm. The results indicate that thicker cold-formed corners and thicker plane plates both exhibit good structural behaviour. But research on the CFCFST columns with carbon steel tubes and wall thickness greater than 6mm, stiffened or not, is still very scarce.

The main objective of this study is to investigate the effect of the stiffener arrangements on the strength, stiffness and ductility of the CFCFST members with cold-formed carbon steel tubes having thicker walls. A total of 30 CFCFST stub columns using cold-formed carbon steel, with tubular thickness of 6mm and 10mm, were constructed and tested under axial compression. As composite compression members, the steel contribution ratio (δ) of the specimens falls well within the provision of Eurocode 4 [24]. Stiffened sections with different stiffener number and width were designed to investigate the effects of the stiffeners on the mechanical behaviours of the CFCFST columns. Normal concrete and self-consolidating concrete with nominal compression strength of 30MPa were used to fill the steel tubes. The equivalent compressive strength, the normalised compressive strength ratio and the predicted capacities using various

design codes, namely AISC [25], BS5400 [26], EC4 [24], and DBJ [27], were all analysed via ignoring the effect of the infilling concrete to the CFCFST specimens. FE model analysis has been conducted to produce complete axial load versus strain curve of the stiffened CFCFST members and provide further insight into the effect of the stiffeners.

2 Experimental programme

2.1 General

A typical stub column specimen configuration, with a length of 600mm and a cross-section of 200×200mm, was used in the CFCFST column tests. The parameters under investigation included: a) Two different tube thicknesses of 6mm and 10mm, with nominal yield strength of 345MPa and 235MPa, respectively. b) Three different types of concrete, namely normal concrete (CC), self-consolidating concrete mix-1 (SCC1) and self-consolidating concrete mix-2 (SCC2), that were used to fill the tubes. The nominal concrete compressive strength was chosen to be 30MPa uniformly. c) Five different cross-section designs, including unstiffened and stiffened cross-sections with different arrangement of the stiffeners.

The detailed configurations of the tubular cross sections of the composite stub columns are shown in Fig. 2. Thus, totally 30 stub column specimens were fabricated and tested. These specimens were classified into 6 groups according to the two wall thicknesses and three types of concrete. Each group included five specimens of different cross section details. A summary of the 6 groups of the specimens is given in Table 1. The specimen labels in Table 1 are defined according to the section configuration, wall thickness, and the type of concrete. Take specimen "Pa-6-1" as an example, (1) "Pa" indicates section "a" as shown in Fig. 2 (a); the five sections are indicated by "Pa" to "Pe" sequentially, (2) the number "6" that follows indicates the thickness of the SHS tubes, "6" means 6mm, and "10" means 10mm, (3) the number "1" next indicates the type of concrete; "1" means normal concrete, "2" SCC1, and "3" SCC2.

Also listed in Table 1 are the measured parameters. B, t_1, and t_2 are the measured average total width of steel tube, average thickness of the plane plates, and average thickness of the corners, respectively. b_s and t_s are the measured average width and thickness of the inner stiffeners, respectively. The definitions of B, t_1, t_2, b_s, and t_s are shown in Fig. 2. A_s is the sectional area of net steel SHS tube including the inner stiffeners, and A_c is the net sectional area of concrete.

The actual strengths of the steel and the concrete materials were determined by standard steel

coupon tests and concrete compression tests, respectively, as described in what follows.

2.2. Properties of steel

Plates cut from the planar parts, the welded parts, and the corner parts of the hollow tubular sections as well as plates from the inner stiffeners were all processed into short standard tensile coupons, according to standard procedures [28]. Totally eight groups of steel tensile coupons, with three coupons in each group, were tested. The average sectional areas (A_P) are listed in Table 2. The average ultimate strength (σ_u) and average yield strength ($\sigma_{0.2}$) for each group as obtained from the coupon tests are also listed in Table 2.

It is noted that in Table 2, "PP", "WP", "CP", and "SP" indicate coupons from the planar area, welded area, corner area, and inner stiffener area of the cold-formed section, respectively. The number of "6", "10", and "8" refer to the nominal thickness of the coupons. It can be observed that the actual strength of the steel, as represented by $\sigma_{0.2}$ of PP-6 (438 MPa) and PP-10 (382MPa), was apparently higher than the nominal yield strength of 345 and 235MPa, respectively. The strength $\sigma_{0.2}$ of coupons CP-6 and CP-10, being 540 and 434MPa, were even higher due to the cold-formed fabricating process. The strengths of the WP coupons were also influenced significantly by the welding process. More details of the coupon tests can be found in reference [23].

2.3. Concrete mix designs and measured concrete properties

The concrete mix was designed to achieve a 28-day compressive cube strength of 30MPa. Ordinary Portland cement and fly ash of Class-F in Level-II were used to make the infilling concrete. To evaluate the effects of the properties of the concrete on the axial compressive behaviour of the CFST columns, three different mix designs, namely CC, SCC1, and SCC2 as mentioned before, were considered and the corresponding mix proportions are shown in Table 3. The same type of aggregates was used in all concrete designs. The aggregate size ranged in 5~25mm. Small quantities of cement expansive additive UEA were mixed into the CC and SCC1 mixes but not into the SCC2 mixes, while small quantities of high strength water reducer HL-8000 were mixed into the SCC1 and SCC2 mixes.

Standard cube specimens of dimensions 150×150×150mm and prismoid specimens of dimensions 150×150×300mm were prepared and tested to obtain the actual concrete properties. The measured compressive cube strength and Young's modulus at 28 days are also presented in

Table 3. The average strengths of CC, SCC1, and SCC2 samples were 26.6, 25.8, and 24.5MPa, respectively. The corresponding Young's modulus values were 31.2, 28.4, and 27.8GPa, respectively. Slightly reduced compressive strength and Young's modulus occurred in the SCC samples, and this may be attributed to presence of super plasticizer. Typical failure modes of the cube and prism specimens are shown in Fig. 3.

2.4 Verification of the CFCFST column design and fabrication of column specimens

As mentioned in Section 2.1, six groups of column specimens were included in the tests. In this section, the details of the CFST properties are explained and discussed.

For an assessment of the potential of local buckling in a CFST member, a width-to-thickness ratio parameter R is commonly used, and the R parameter for concrete infilled specimens with unstiffened sections and stiffened sections which have four stiffeners can be obtained by the following equation [4]:

$$R = \frac{b}{t}\sqrt{\frac{12(1-\nu^2)}{\pi^2 k}}\sqrt{\frac{\sigma_y}{E}} \qquad (1)$$

where b/t is the ratio of width to thickness of SHS tube, E and ν are Young's modulus and Poisson's ratio of steel and are assumed to be 200GPa and 0.3, respectively. σ_y is the yield stress of steel. k is the buckling coefficient, $k = 4n^2$, where $n = 1$ and 2 for unstiffened section and stiffened section with one stiffener on each wall.

For the specimens with 6mm-thick tubes, the values of R are calculated to be 0.8 and 0.4 for unstiffened sections and stiffened sections with four stiffeners, respectively. For specimens with the 10mm-thick tubes, the corresponding values are respectively 0.4 and 0.23. All of these R values are below the limiting value of 0.9 concerning local plate [5]. The width-to-thickness ratios b/t for specimens with 6mm- and 10mm-thick tubes are about 33 and 20, which are respectively below the limits of 38 and 40 calculated using $52(235/\sigma_y)^{0.5}$ in EC4 [24].

According to the EC4, the measured steel contribution ratios δ of all specimens range from 0.69 to 0.81 as shown in Table 1, which meet the given limiting range of $0.2 \leq \delta \leq 0.9$. The thickness of the inner stiffeners in the thinner and thicker tubes was 6 and 8mm, respectively. With reference to Fig. 2, two stiffeners with a width of 40 and 60mm were used in the sections C and D, respectively. The stiffener rigidity of these specimens can be calculated as $I_s = b_s \cdot t_s^3/12$, and the

results are listed in Table 4. b_s and t_s are the measured width and thickness of the stiffeners as reported in Table 1. According to reference [8], the minimum required stiffener rigidity can be calculated using either of the equations:

$$I_{s1} = 3.1\times10^4 \cdot (w/t)^{3.5} \cdot (f_{yt}/280) \cdot t^4 \qquad (2)$$

$$I_{s2} = 0.045 \cdot (w/t)^2 \cdot (f_{yt}/280) \cdot t^4 \qquad (3)$$

where w is the width of the sub-panel plate, and can be taken approximately as half of the test overall width (B/2). t is the tubular thickness of the specimens, and was given as the measured plate thickness t_1. f_{yt} is the test yield stress of the planar plate, and was given as the test strength $\sigma_{0.2}$ of the planar plates.

The calculated rigidity requirements I_{s1} and I_{s2} are also listed in Table 4. As can be seen, except Pc-10-1, Pc-10-2 and Pc-10-3 which had the stiffener rigidities below the calculated rigidity I_{s2} but still greater than I_{s1}, the stiffener rigidities of all other specimens are greater than both calculated rigidity requirements.

All the unstiffened and stiffened SHS tubes were fabricated in a roll-forming steel plant. Butt welds and fillet welding were applied to build up the tubular wall and the inner stiffeners. For each SHS tube, a bottom plate of plan dimension 240×240mm was welded to one end of the tube in the laboratory. The thickness of the bottom plate was 10mm for the 6mm-thick SHS tubes and 16mm for the 10mm-thick tubes.

Casting of normal concrete filled specimens was done by filling the concrete into the tube in layers, accompanied by manual compaction (vibrating and knocking the tube wall) to consolidate the concrete during the casting. For the self-consolidating concrete filled specimens, the SCC1 and SCC2 concretes were filled in layers only, with limited knocking where needed. These column specimens were then placed upright to air-dry until testing. A small amount of cement mortars was used to fill the slight gap caused by the concrete shrinkage during the curing period, so that the concrete surface was smooth at the top. A top plate with the same thickness and plan dimension as the bottom plate was finally welded about 14 days after the tubes were filled with concrete.

2.5 Testing of the CFCFST columns

The CFST column specimens were tested under axial compression. A compression testing

machine with a design capacity of 5000kN was used to apply the axial compressive load. The axial compression test was designed to determine the axial bearing capacities and failure patterns of the CFCFST columns. Two displacement meters were used to measure the relative displacements between the top and bottom plates. Four longitudinal strain gauges were installed at the mid-height and mid-width to measure the axial strain of the steel tubes. Preliminary test within the elastic range was first conducted. Adjustment of the position of the specimen was carefully made on the basis of the measured four strains to ensure satisfactory uniaxial loading. The adjustment was finalized when the maximum difference between an individual strain and the average strain was no greater than 5%.

As an initial estimation for the planning of the loading scheme, a simplified equation, $N_0 = f_c \cdot A_c + f_{yt} \cdot A_{st} + f_{ys} \cdot A_{ss}$, was used to estimate the axial strength capacity of the CFCFST columns considering the effects of the longitudinal inner stiffeners. In this equation, A_c, A_{st}, and A_{ss} are the measured sectional areas of concrete, the steel tube and the steel stiffeners, respectively. The total measured sectional area of the steel, including both the tube and stiffener net sectional area, is also reported in Table 1, along with the measured yield strengths of the steel tube ($f_{y,t}$) and the steel stiffeners (f_{ys}). Table 2 list the concrete strength properties, where f_c is the characteristic concrete strength and may be calculated as f_c=0.67·f_{cu}, and f_{cu} is the test cube strength of the concrete.

Considering the estimated capacities, a load interval of 250kN was chosen in the test for all specimens. Each load interval was maintained for about 3 minutes. Test capacity of all specimens was reported in Table 1. A typical CFCFST column test setup is shown in Fig. 4.

3 Experimental results of CFCFST columns and analysis

3.1 Rigidity, strength, ductility and failure mode

Figs. 5 and 6 show the axial load (N) versus average steel strain (ε_s) curves of specimens with 6mm- and 10mm-thick steel tubes, respectively. It is noted that all the specimens failed with buckling of the steel tubes when the peak load was reached, which was characterised by a rapid decline in the load carrying capacity accompanied by large axial deformation. Therefore, no detail of the descending branch was captured during the test. A few specimens, in particular the Pd-10-2, Pe-10-1 and Pe-10-2 which had the thicker tubes along with the largest stiffening effect, did not reach the peak load due to the limiting load capacity of the test setup. Shown in Fig. 5

and 6 are also the axial load vs. steel strain curves form the finite element analysis, which will be discussed in more detail in Section 5 later.

All N-ε_s curves exhibit good linear behaviour during the initial loading stage, and generally speaking the rigidity (slope of the N-ε_s curve) of the specimens did not appear to be affected significantly by the sectional configurations. However, the gross axial load capacity N_{ue} tended to increase markedly with increase of the stiffener area in a sequential order from sectional type "a" to "e", as shown in both the curves and Table 1. Compared with the corresponding specimens with sectional type "a", the increase degree of capacity N_{ue} of specimens Pc-10-1, Pc-10-2 and Pc-10-3 is less than specimens with tubular thickness of 6mm. One possible reason is that the calculated stiffener rigidities of specimens Pc-10-1, Pc-10-2 and Pc-10-3 are even less than the rigidity requirements I_{s2}, as mentioned in Section 2.4. The capacity N_{ue} also increased with increase of the wall thickness from 6mm to 10mm, as can be expected. More detailed analysis of the variation in strength will be discussed later in Section 3.2. Despite that the whole loading-deformation curve was not obtained for most of the specimens, the general deformability from the start of apparent nonlinear response towards the maximum load can still be observed from Figs. 5 and 6. For specimens with more stiffeners or wider stiffeners, the deformability tended to be better. The CC, SCC1, and SCC2 concrete samples were obtained using different mix proportions, but the test cube strengths were close. The effect of the mix HL-8000 and UEA on the capacity was insignificant.

Fig. 7 shows typical failure modes for specimens with 6mm- and 10mm-thick steel tubes, respectively. Except the few specimens with 10-mm thick tubes and sectional configurations "d" and "e" which did not produce a failure pattern for the reasons explained before, the following observation can be made:

(1) For specimens with unstiffened steel sections, significant outward buckling similar to the Fig. 8 (a) occurred. The buckling took place near the upper (loading) end. This may be explained by the fact that it was impossible to achieve a perfectly intact and uniform state of concrete infill at the upper end.

(2) For specimens with Section type-b shown in Fig. 2, i.e. with a total of two stiffeners, outward buckling occurred at several locations in the steel plates from the unstiffened specimens, and local buckling occurred earlier in the two unstiffened walls of the tube than in the stiffened walls. At the end of loading process, the buckling deformation of the unstiffened walls was significantly larger than that of the stiffened walls. The unstiffened plate of the specimen Pb-6-2

even cracked along the central weld due to the large buckling deformation as shown in Fig. 7(b). The effectiveness of the stiffeners in postponing the buckling of the steel plates was clearly demonstrated.

(3) Failure modes of specimens with Section type-c were still featured by a rather concentrated major longitudinal buckling. However the severity of buckling was much reduced due to the addition of stiffeners on all four sides of the steel tubes. As a result the maximum load generally increased as compared to Section type-a and type-b.

(4) Specimens with Section type-d had wider stiffeners with a width of 60mm as compared to 40mm in Section type-c. In these specimens, major longitudinal buckling tended to be effectively suppressed, and instead, local buckling occurred in multiple locations and between the adjacent stiffeners. Clearly, the rigidity of the stiffeners influenced the failure modes. As mentioned earlier, the rigidities of both the 40mm- and 60mm-wide stiffeners satisfied the requirements as calculated using either Eq. (2) or Eq. (3). However, only the failure modes of the specimens with the wider stiffeners appeared to have effectively prevented an undesired "global" buckling. Thus the wider stiffeners enabled a fuller development of the capacities both in the steel tubes and in the concrete under the confinement of the steel tubes. The failure modes in the Section type-d specimens echoed well the more favourable failure modes obtained in some previous studies [4, 8] as shown in Fig.8 (b). Based on the above observations, modifications of Eqs. (2) and (3) are deemed to be necessary in order to prevent an undesirable "global" style of buckling in the stiffened CFCFST specimens.

(5) With the further enhancement of the stiffening effect as in the cases of Section type-e specimens, buckling appeared to be effectively controlled, and as a result the load carrying capacities of these specimens were the largest among the specimens of the same wall thickness.

(6) No cracks have been found at the cold-formed corners during the test process of all specimens, which shows that the round cold-formed corners have good mechanical behaviour under the axial compression.

3.2 Further analysis on the effect of stiffeners

According to Figs. 5 and 6, the average sectional stress (f_{sc}) versus axial steel strain ($\varepsilon_{s,av}$) curves of specimens with the same sections were analyzed. In order to simplify the analysis, the effect of the concrete mix HL-8000 and UEA of the infilling concrete was ignored in this section. Figs. 9 (a) and (b) are the f_{sc} versus $\varepsilon_{s,av}$ curves of specimens with 6mm- and 10mm-thick tubes,

respectively. f_{sc} is the sectional stress corresponding to the recorded load during the test proceeding, and can be obtained via dividing the recorded load by average overall sectional area of the three specimens which have same nominal sections. $\varepsilon_{s,av}$ is the average measured steel strain of the three specimens, and can be obtained from the measured strains of the corresponding specimens.

From Figs. 9 (a) and (b), all the f_{sc} versus $\varepsilon_{s,av}$ curves exhibit a strain hardening stage after the elastic-plastic stage, although the confinement factors $\xi = (f_{yt} \cdot A_{st} + f_{ys} \cdot A_{ss})/(f_{ck} \cdot A_c)$ [29] of many specimens did not indicate a hardening response. In fact, the confinement factors in sections "a", "b" and "c" and in all the 6mm-thick tubes ranged from 3.34 to 4.29 (Table 1), which are less than the factor ξ_0. ξ_0 is a critical factor defining whether or not a CFST member would have a harden stage and is given as 4.5 [29]. The strength f_{ck} here equals to the strength mentioned in Section 2.5. Thus the core concrete tends to be confined more effectively with SHS tubes of 6mm wall thickness in both stiffened and unstiffened cases than with normal thin-walled SHS steel tubes. For specimens with both 6mm- and 10mm-thick tubes, the f_{sc} versus $\varepsilon_{s,av}$ curves appeared to go upwards significantly when more stiffeners or wider stiffeners were used, indicating a significant enhancement of the ultimate capacity in these cases.

From the gross axial load capacity (N_{ue}), an equivalent compressive strength for the composite material in the cross-section (f_{ue}) can be calculated as follows:

$$f_{ue} = \frac{N_{ue}}{A_s + A_c} = \frac{N_{ue}}{A_{sc}} \qquad (4)$$

where A_s and A_c are the measured sectional area of steel and concrete, respectively. The calculated equivalent compressive strength f_{ue} of the specimens were also listed in Table 1. As a reference, the nominal equivalent strength of the cross-section based on the yield strength of steel and the compressive strength of the concrete is also calculated for a comparison, as

$$f_{ue,0} = \frac{f_{ys} A_s + f_c A_c}{A_s + A_c} = \frac{N_0}{A_{sc}} \qquad (5)$$

A normalised compressive strength ratio can then be defined to measure the overall effectiveness of the CFCFST composite column, as

$$\eta_f = \frac{f_{ue}}{\bar{f}_{ue,0}} \qquad (6)$$

It is understood that the load capacity of the CFCFST sections depends upon the effective contribution of the steel area (tube and stiffeners) in undertaking the compressive force, as well as the strength of the concrete under the confinement of the steel tubes. Generally speaking, it may be expected that the direct and indirect (through confinement) contributions of steel would be in line with each other and therefore produce a compounded effect.

In order to examine further the effect of the inner stiffeners on the composite action between the steel tube and core concrete, the average equivalent compressive strength ($f_{ue,av}$) and normalised compressive strength ratio ($\eta_{f,av}$) of specimens with same sections were also analyzed. The results are given in Table 5. Here, the average confinement factor ξ_{av} of the specimens with the same sections are considered, and the $f_{ue,av}$ - ξ_{av} and $\eta_{f,av}$ - ξ_{av} curves of the specimens are shown in Figs. 10 and 11, respectively.

As can be seen from Fig. 10, as the factor ξ_{av} increases, the stress $f_{ue,av}$ of specimens with both 6mm- and 10mm-thick tubes increase significantly. However, it can be observed that the increase of the stress $f_{ue,av}$ of specimens with 10mm-thick tubes tends to be less comparing to specimens with 6mm-thick tubes. This indicates that the effect of the number and width of stiffeners on the ultimate sectional stress is less significant in specimens with thicker tubes than in specimens with thinner tubes. From Fig. 11, the average ratio $\eta_{f,\mathrm{av}}$ among specimens with 6mm-thick tubes appears to be increasing as the factor ξ_{av} increases. The ratios for specimens with sections “a”, “c”, and “e” are 1.08, 1.20 and 1.30, which shows that the number of stiffeners affects this ratio significantly when the tubular walls are equally stiffened. Meanwhile, the ratio can also be increased by using wider stiffeners, as it can be seen that the ratio of specimens with section “d” is 1.29.

4. Comparison of predicted and test strengths

There are several widely used design codes for predicting the capacity of CFST columns. In this study, the methods in the codes AISC [25], BS5400 [26], EC4 [24], and DBJ [27] have been employed to predict the strength capacities of the CFCFST specimens and compared with the experimental results.

AISC [25] specifies a limiting slenderness parameter, λ_p, for compact plates, and it is calculated

as $\lambda_p = 3.0(E_s / f_y)^{0.5}$. The present test specimens had E_s = 200GPa and the yield strengths equal to 438MPa and 382MPa for the 6mm- and 10mm-thick wall tubes, respectively. The limiting values of λ_p are found to be much greater than the actual width-to-thickness ratios of the specimens. Therefore the sectional strength can be calculated as $N_{AISC} = f_y A_s + 0.85 f_c' A_c$, where A_s and A_c are total sectional area of steel and sectional area of concrete, respectively; f_y and f_c' are the yield stress of steel and the compressive strength of concrete, respectively. Herein f_y is assumed to be the test strength $\sigma_{0.2}$ shown in Table 2, and f_c' is calculated as $0.4 \cdot (f_{cu})^{7/6}$ [8], where f_{cu} are the test concrete cubic strength shown in Table 3.

BS5400 [26] defines the quash load for composite cross sections, which can be calculated as $N_{BS5400} = f_y \cdot A_s + 0.675 f_{cu} \cdot A_c$, where f_{cu} is the cube strength of concrete as given in Table 3. In EC4 [24], the nominal strength for composite compression columns is given as $N_{EC4} = f_y \cdot A_s + f_{cd} \cdot A_c$, where f_{cd} is the design value of the cylinder compressive strength of concrete, and is herein assumed as the same value as the strength f_c' mentioned in the AISC specification.

According to the DBJ 1351-2003 [27], the squash load of the composite section can be calculated as $N_{DBJ} = (1.18 + 0.85 \cdot \xi) \cdot f_{ck} \cdot A_{sc}$, where ξ is the confinement factor mentioned in Section 3.2. The average ratios of the predicted to the test strengths are presented in Table 6, ignoring the influence of the infilling concrete. The average ratio versus ξ_{av} curves are shown in Fig.12.

From Table 6 and Fig. 12, several observations can be made as follows:

(1) For specimens with 6mm-thick tubes, the ratios N_{AISC}/N_{ue}, N_{BS5400}/N_{ue}, N_{EC4}/N_{ue}, and N_{DBJ}/N_{ue} are less than 1.0 and decrease significantly with factor ξ_{av}. It demonstrates that the above code methods are more conservative in predicting the strength capacity of the test specimens with more or wider inner stiffeners. Except Pd-10 and Pe-10 specimens, for which the recorded strength capacities were less than the actual ultimate capacities for reasons mentioned in Section 3.1, most ratios for specimens with 10mm-thick tubes are less than 1.0. The ratios of Pc-10 specimens are even greater than Pa-10 and Pb-10 specimens. Hence the code methods tend to be less conservative in predicting the strength capacities of Pc-10 test specimens. Excluding this, the code methods tend to be more conservative in predicting the ultimate strengths of Pa-10 and Pb-10 specimens than those of Pa-6 and Pb-6 specimens. The possible reason is that the presence of inner stiffeners affected the capacity of specimens with thinner wall tubes more significantly

than with the thicker wall tubes, as mentioned in Section 3.

(2) As can be seen from Section 4.1, the difference in the corresponding ratios N_{AISC}/N_{ue}, N_{BS5400}/N_{ue}, and N_{EC4}/N_{ue} is attributable to the difference in the concrete strengths used in the calculation. Comparatively speaking, the EC4 method appears to be the least conservative as the corresponding ratios are the closest to 1.0 among the three code methods. For specimens with accurate recording of the actual ultimate capacities, the DBJ code appears to be the best method to predict the test capacity, especially for those specimens with unstiffened or less stiffened sections.

5. Finite element analyse and comparison with test results

To assist in the interpretation of the test results and extend the examination into the underlying mechanics of the CFCFST stub columns, a finite element study has been conducted on the specimens using the general purpose FE software ABAQUS. In the FE model, shell element C4R and solid element C3D8R were used to model the steel tube and in-fill concrete, respectively. The two end-plates were simplified as rigid plates and modeled using the discrete rigid body element R3D4, and attached to the steel tube via shared nodes at the adjoining points. In order to model the boundary conditions in the test (see Fig.4), the bottom plate was assumed as being fully restrained while the top plate was loaded in the vertical direction. The interface between the steel tube and the in-fill concrete was modelled as surface-to-surface and hard contact in the normal direction. Penalty friction formula with bond-slip was used to model the tangential friction of the interfaces.

An equivalent stress-strain relationship of confined concrete [30] and a plastic damage model [31-32] were considered to define the constitutive properties of the in-fill concrete. The damage factor was defined according to the recommendations in [33]. The ultimate compressive stress f_{cu} listed in Table 3 was applied. The concrete tensile strength and the fracture energy G_F were defined according to Tao et al. [34]. The "yield" stress was chosen as $0.1f_{cu}$. A multi-linear stress versus strain curve for the cold-formed steel, introduced in [35], was used to simulate the material property of the steel tubes. The average test yield ($\sigma_{0.2}$) and ultimate (σ_u) stresses of the planar, welded, corner and stiffener coupons reported in Table 2 were used to predict the steel stress-strain curve of the corresponding sectional parts. The reference Young's modulus E_s and Poisson's ratio of the steel tube were assumed to be 2.06×10^5 MPa and 0.3, respectively.

The eigenvalue buckling analysis of the SHS column specimens was conducted. Initial geometric

imperfection with the same distribution as the first-order eigenvector was introduced to the corresponding FE model to simulate the local buckling, where the maximum size of the imperfection was set to one-tenth of the corresponding wall thickness [36]. The material strength was governed by the Mises Yield Criterion.

In order to obtain an appropriate element mesh size, the FE model of Specimen Pa-6-2 was analysed using three element sizes of 20mm, 15mm and 10mm. The calculated sectional capacities $N_{u,FEA}$ were 2772kN, 2801kN and 2814kN, respectively. The results can be considered as stable with all these mesh sizes. The predict capacity 2801kN is 6.94% less than the test capacity 3010kN. The final element size was chosen to be 15mm for the FE model of of the column specimens.

As an example, Table 7 lists the FE analysis results for the second group of specimens named as "-2" in Table 1, including the predicted bearing capacity $N_{u,FEA}$, ratio of the predicted bearing capacity shared by the steel tube $N_{ut,FEA}$ to the capacity $N_{u,FEA}$ (i.e. $N_{ut,FEA}/ N_{u,FEA}$), and the predicted average sectional stress $\sigma_{FEA,T}$. The comparison between the FE analysis and the test results are represented by the difference between the bearing capacities obtained from the FE analysis $N_{u,FEA}$ and the test value of N_{ue}, as $\Delta_1=(N_{u,FEA}- N_{ue})/N_{ue}\times100\%$. Similarly, Δ_2 denotes the difference between the stress $\sigma_{FEA,T}$ of steel tubular section 'b' to 'e' and section 'a' of the test counterparts. The force-strain curves obtained from the FE analysis have been included in Figs. 5 (b) and 6(b) along with the experimental curves. Typical predicted failure patterns are shown in Fig.13.

As can be seen from Figs. 5 (b) and 6(b), during the initial loading stage, the predicted σ-ε_s curves agree well with the measured curves. In terms of the predicted ultimate capacity marked with symbol "•" in Figs. 5 (b) and 6(b) and also listed in Table 7, the FEA analysis result agree with the measured result well. Compared with the measured capacity N_{ue}, the predicted capacity $N_{u,FEA}$ is less for specimens with 6mm-thick tubes while fluctuates up and down for specimens with 10mm-thick tubes. The difference Δ_1 ranging from -6.94% to 6.92%. Considering the fact that the measured bearing capacities of specimens Pc-10-2, Pd-10-2 and Pe-10-2 were somewhat less than their real capacities because of the missing peak loads, the predicted results matched the test results actually even better. Also from Figs. 5(b) and 6(b), for specimens with 6mm-thick tubes, the strain corresponding to the maximum load increases with the number or the width of the stiffeners. The confining factor of specimens with 10mm-thick tubes is larger (greater than 4.5) so that the curves of Pc-10-2, Pd-10-2 and Pe-10-2 rise quite slowly in this nonlinear phase of the curves. The predicted σ-ε_s curves are consistent with the results from [30].

From Fig. 13, the predicted failure modes from the FE model are similar to the corresponding failure modes from the experiment shown in Fig. 7. It should be noted that the failure modes for Pd-10-2 and Pe-10-2 were not available from the experiment, as mentioned in Section 3.1. Significant outward buckling occurred near the loading end of specimen with Section type “a”, while earlier and larger buckling deformations occurred in the unstiffened walls of the specimens with Section type “b”. These are all in agreement with the experimental observations.

6. Conclusions

A total of 30 CFCFST columns with both unstiffened and inner longitudinally stiffened SHS tubes with thicker walls have been tested under axial compression. The effects of the inner stiffeners on the rigidity, ductility, failure mode, and sectional capacity of the specimens have been analysed. The accuracy of using various code methods to predict the strength capacities of these types of CFCFST columns, including AISC [25], BS5400 [26], EC4 [24], and DBJ [27], has been assessed. Furthermore, an FE model has also been developed to analyze the response of the columns. The following main conclusions and suggestions can be drawn:

(1) The rigidity of the specimens is affected insignificantly by the sectional configurations while the ductility tends to increase with the number or width of the inner stiffeners. The round cold-formed corners have good mechanical behaviour under the axial compressive loads and no cracks have been found at the corners. The failure mode is affected obviously by both the number and width of the stiffeners.

(2) Both the overall strength and equivalent compressive strength increase markedly with the sectional area of the inner stiffeners. The increase of strengths in specimens with 6mm-thick tubes are found to be more significant than the increase in the specimens with 10mm-thick tubes. The normalised compressive strength ratio increases more significantly with the inner stiffener number than the width, and the increase of the specimens with 6mm-thick tubes is also more significant than specimens with 10mm-thick tubes. It is recommended that the rigidity of the four inner stiffeners in sectional type “c” should meet the rigidity requirements I_{s2}.

(3) The code methods are found to be more conservative in predicting the strength capacity of the CFCFST specimens with more or wider inner stiffeners, for specimens with 6mm-thick tubes, while tends to be less conservative for specimens with 10mm-thick tubes. The prediction methods in the AISC, BS5400 and EC4 are similarly on the conservative side, and the method in the DBJ code is comparatively the best method for the prediction of the strength capacity of the specimens, especially for those with unstiffened or less stiffened sections.

(4) The FE model has shown satisfactory performance in predicting the bearing capacity, the load and strain curves, as well as the failure modes. Such a model provides a useful means to extend the examination into the underlying damage processes in the CFCFST columns.

As the experimental results have indicated, the effectiveness of increasing the wall thickness in enhancing the combined strength of confined concrete and the steel material has a certain limit. Further research is required in order to establish quantitatively such limit with the consideration of the stiffeners in different profiles. To this end, more detailed finite element analysis is expected to play an important role in addition to extended experimental investigations.

Acknowledgement

The authors are grateful to the supports of National Natural Science Foundation of China (No. 51108204 & No. 51578260) and the Fundamental Research Funds for the Central Universities (No. 2016YXMS095).

References

[1] Tao Z., Han LH., Wang DY. Strength and ductility of stiffened thin-walled hollow steel structural stub columns filled with concrete. Thin-Walled Structures, 2008(46): 1113-1128.

[2] Uy B. Strength of concrete filled steel box columns incorporating local buckling. Journal of Structural Engineering, 2000(126): 341-352.

[3] Uy B. Local and post-local buckling of concrete filled steel welded box columns. Journal of Constructional Steel Research, 1998(47): 47-72.

[4] Ge HB., Usami T. Strength of concrete-filled thin-walled steel box columns: Experiment. Journal of Structural Engineering, 1992(118): 3036-3054.

[5] Ge HB., Usami T. Strength analysis of concrete-filled thin-walled steel box columns. Journal of Constructional Steel Research, 1994(30): 259-281.

[6] Kitada T. Ultimate strength and ductility of state-of-the-art concrete-filled steel bridge piers in Japan. Engineering Structures, 1998(20):347-354.

[7] Liu YJ., Zhang JG., Xu KL., et al. Experimental research on stub columns of concrete-filled steel box with longitudinal stiffener under axial load, Journal of Building Structures. 2011, 32(10): 159-165 (in Chinese).

[8] Tao Z., Han LH., Wang ZB. Experimental behaviour of stiffened concrete-filled thin-walled hollow steel structural (HSS) stub columns. Journal of Constructional Steel Research, 2005 (61): 962-983.

[9] Tao Z., Han LB., Wang DY. Experimental behaviour of concrete-filled stiffened thin-walled steel tubular columns. Thin-Walled Structures, 2007(45): 517-527.

[10]Tao Z., Uy B., Han LH., Wang ZB. Analysis and design of concrete-filled stiffened thin-walled steel tubular columns under axial compression. Thin-Walled Structures, 2009(47): 1544-1556.

[11]Petrus C., Hamid HA., Ibrahim A., Parke GA. Experimental behaviour of concrete filled thin walled steel tubes with tab stiffeners. Journal of Constructional Steel Research, 2010, 66(7): 915-922.

[12]Chitawadagi MV., Narasimhan MC., Kulkarni SM. Axial capacity of rectangular concrete-filled steel tube columns-DOE approach. Construction and Building Materials, 2010(24): 585-595.

[13]Zhang YC., Chen Y. Experimental study and finite element analysis of square stub columns with straight ribs of concrete-filled thin-walled steel tube. Journal of Building Structures, 2006, 27(5):16-22 (in Chinese).

[14]Zhang Y., Xu C., Lu XZ. Experimental study of hysteretic behaviour for concrete-filled square thin-walled steel tubular columns. Journal of Constructional Steel Research, 2007(63): 317-325.

[15]Young B., Ellobody E. Experimental investigation of concrete-filled cold-formed high strength stainless steel tube columns. Journal of Constructional Steel Research, 2006(62): 484-492.

[16]Ellobody E., Young B. Design and behaviour of concrete-filled cold-formed stainless steel tube columns. Engineering Structures, 2006(28): 716-728.

[17]Uy B., Tao Z., Han LH. Behaviour of short and slender concrete-filled stainless steel tubular columns. Journal of Constructional Steel Research, 2011(67): 360-378.

[18]Guo YJ., Zhu AZ., Pi YL., et al. Experimental study on compressive strengthen of thick-walled cold-formed sections. Journal of Constructional Steel Research, 2007(63): 718-723.

[19]Chan TM., Huai YM., Wang W. Experimental investigation on lightweight concrete-filled cold-formed elliptical hollow section stub columns. Journal of Constructional Steel Research, 115 (2015): 434–444.

[20]Afshan S., Rossi B., Gardner L. Strength enhancements in cold-formed structural sections-Part I: Material testing. Journal of Constructional Steel Research 2013(83):177-188.

[21]Tong LW., Hou G., Chen YY., et al. Experimental investigation on longitudinal residual stresses for cold-formed thick-walled square hollow section. Journal of Constructional Steel Research, 2012(73):105-116.

[22]Hu SD., Ye B., Li LX. Materials properties of thick-wall cold-rolled welded tube with a rectangular or square hollow section. Construction and Building Materials, 2011(25):2683-2689.

[23]Zhu, AZ., Zhu, HP., Zhang, XW., Lu, Y. Experimental study and analysis of inner-stiffened cold-formed SHS steel stub columns. Thin-Walled Structures, 107 (2016): 28-38

[24]Eurocode 4. Design of composite steel and concrete structures, Part1.1, general rules and rules for building. London: British Standards Institution; 2004 (BS EN 1994-1-1: 2004).

[25]ANSI/AISC 360-05. Specification for structural steel buildings. American Institute of Steel Construction. Chicago, USA; 2005.

[26]BS5400. Steel, concrete and composite bridges, Part 5, Code of practice for the design of composite bridges. London, UK; 2005.

[27]DBJ13-51. Technical specification for concrete-filled steel tubular structures. Fuzhou, China: The Construction Department of Fujian Province; 2003(in Chinese).

[28]Tang YQ., Ye WM. A handbook of testing technique in civil engineering. Shanghai, China: Tongji University Press; 1999 (in Chinese).

[29]Han LH., Yao GH., Zhao XL. Tests and calculations for hollow structural (HSS) stub columns filled with self-consolidating concrete (SCC). Journal of constructional Steel Research, 2005(61): 1214-1269.

[30]Han LH. Concrete-filled steel tube structure: theory and practice. Beijing, China: Science Press; 2004(in Chinese)

[31]Lubliner J, Oliver J, Oller S, Onate E. A plastic-damage model for concrete[J]. International Journal of Solids and Structures, 1989 (25):299-326.

[32]Lee J., Fenves. GL. Plastic-Damage model for cyclic loading of concrete structures. Journal of Engineering Mechanics, 1998 (8): 892-900.

[33]ABAQUS Users' Conference. 2006.

[34]Tao Z, Wang ZB, Yu Q. Finite element modelling of concrete-filled steel stub columns under. Journal of Constructional Steel Research, 2013(89):121-131.

[35]Abdel-Rahman N, Sivakumaran KS. Material properties models for analysis of cold-formed steel members. Journal of Structural Engineering, 1997(123): 1135-1143.

[36]Chinese Standard (GB) 50018. Technical code of cold-formed thin-wall steel structures. China; 2002 (in Chinese)

Table 1

Specimen labels, measured dimensions and section capacities

Specimen label	B (mm)	t_1 (mm)	t_2 (mm)	b_s (mm)	t_s (mm)	A_s (mm^2)	A_c (mm^2)	δ	ξ	N_{ue} (kN)	f_{ue} (MPa)
Pa-6-1	197.0	6.4	6.2	0	0	4704	33880	0.70	3.41	2730	70.75
Pb-6-1	200.0	6.1	6.3	40	6.26	5088	34683	0.71	3.59	3020	75.93
Pc-6-1	197.5	6.2	6.2	40	6.09	5598	33222	0.74	4.10	2750	70.84
Pd-6-1	199.0	6.1	6.2	60	6.03	6033	33361	0.75	4.38	4120	104.58
Pe-6-1	201.5	6.2	6.0	40	6.09	6653	33706	0.77	4.77	4490	111.25
Pa-6-2	198.5	6.1	6.3	0	0	4565	34577	0.69	3.34	3010	76.90
Pb-6-2	200.5	6.1	6.0	40	6.08	5082	34873	0.71	3.67	3300	82.59
Pc-6-2	198.5	6.1	6.1	40	6.00	5557	33650	0.74	4.14	3630	92.59
Pd-6-2	198.0	6.1	6.2	60	5.95	5984	33005	0.75	4.52	4030	103.30
Pe-6-2	202.0	6.2	6.1	40	6.28	6604	33497	0.77	4.90	4300	107.23
Pa-6-3	200.5	6.3	6.2	0	0	4730	35237	0.70	3.59	2830	70.81
Pb-6-3	199.0	6.1	6.0	40	6.68	5086	34305	0.72	3.93	3030	76.92
Pc-6-3	200.5	6.1	6.3	40	6.22	5584	34397	0.73	4.29	3520	88.04
Pd-6-3	199.5	6.4	6.5	60	6.04	6240	33361	0.76	4.92	3960	100.00
Pe-6-3	201.5	6.1	6.3	40	6.02	6579	33790	0.77	5.11	4550	112.71
Pa-10-1	201.0	10.3	10.1	0	0	7467	32328	0.73	4.95	3980	100.01
Pb-10-1	200.0	10.2	10.0	40	8.80	8085	31400	0.76	5.61	4510	114.22
Pc-10-1	198.5	10.1	10.1	40	7.96	8600	30356	0.78	6.24	4500	115.51
Pd-10-1	198.5	10.0	10.2	60	8.20	9219	29682	0.80	6.92	4400	113.11
Pe-10-1	200.5	10.0	9.8	40	8.26	9913	29729	0.81	7.51	4700	118.56
Pa-10-2	201.0	10.0	10.2	0	0	7328	32536	0.72	4.97	3920	98.33
Pb-10-2	201.0	10.2	10.2	40	8.24	8058	31784	0.75	5.68	4330	108.68
Pc-10-2	200.5	10.1	10.1	40	7.90	8645	31167	0.77	6.29	4340	109.01
Pd-10-2	199.0	10.1	9.9	60	7.83	9139	29977	0.79	6.99	4550	116.32
Pe-10-2	200.5	10.1	10.1	40	8.32	9939	29632	0.81	7.78	4625	116.88
Pa-10-3	199.5	10.1	9.9	0	0	7283	31964	0.73	5.30	3900	99.37
Pb-10-3	199.0	10.2	10.1	40	8.64	8067	31070	0.76	6.14	4390	112.17
Pc-10-3	198.0	10.1	10.2	40	8.22	8609	30156	0.78	6.84	4430	114.28
Pd-10-3	199.0	10.1	10.1	60	8.00	9202	29934	0.80	7.44	4550	116.26
Pe-10-3	200.0	10.1	9.8	40	8.02	9876	29618	0.81	8.14	4700	119.01

Table 2
Test strength of the tensile coupons

Specimen	A_P (mm^2)	σ_u (MPa)	$\sigma_{0.2}$ (MPa)
PP-6	221.51	537.37	437.88
WP-6	212.57	582.00	535.54
CP-6	94.62	614.00	539.76
S-6	186.73	531.63	410.79
PP-10	341.61	445.67	381.68
WP-10	359.20	526.93	505.00
CP-10	318.34	495.47	433.55
SP-8	244.30	551.07	453.59

Note:
(1) “PP”, “WP”, “CP”, and “SP” indicate coupons from the planar coupons, welded coupons, corner coupons, and inner stiffener coupons cut from the cold-formed section, respectively.
(2) “6”, “10”, and “8” refer to the nominal thickness of the coupons.

Table 3
Concrete mix design and test results

Material	Content (kg/m^3)		
	CC	SCC1	SCC2
Sand (%)	50%	50%	50%
Cement	256	256	256
Flash ash	86	86	86
Water	200	200	200
Sand	909	909	909
Aggregate	909	909	909
UEA	38	38	0
HL-8000	0	3.8	3.4
f_{cu} (MPa)	26.58	25.81	24.47
E_c($\times 10^4$ MPa)	3.12	2.84	2.78

Table 4
Measured stiffener rigidity and calculated rigidity requirements

Specimen label	I_s (mm^4)	I_{s1} (mm^4)	I_{s2} (mm^4)
Pc-6-1	32480	11555	26387
Pd-6-1	108540	11769	25932
Pc-6-2	32000	11665	25802
Pd-6-2	107100	11563	25672
Pc-6-3	33173	12082	26324
Pd-6-3	108720	12161	28689
Pc-10-1	42453	13091	61691
Pd-10-1	147600	13026	60475
Pc-10-2	42133	13559	62940
Pd-10-2	140940	13207	62002
Pc-10-3	43840	12976	61381
Pd-10-3	144000	13207	62002

Table 5
Measured stiffener rigidity and calculated rigidity requirements

Specimen		$\eta_{f,av}$	ξ_{av}	$N_{ue,av}$ (kN)	$f_{ue,av}$ (MPa)
CFST-6	Pa-6	1.08	3.45	2856.67	72.82
	Pb-6	1.10	3.73	3116.67	78.48
	Pc-6	1.19	4.21	3575.00	90.31
	Pd-6	1.26	4.61	4036.67	102.65
	Pe-6	1.29	4.92	4446.67	110.40
CFST-10	Pa-10	1.17	5.08	3933.33	99.24
	Pb-10	1.20	5.81	4410.00	111.69
	Pc-10	1.13	6.46	4423.33	112.94
	Pd-10	1.08	7.12	4500.00	115.23
	Pe-10	1.04	7.81	4675.00	118.15

Table 6
Comparison of predicted and experimental section capacities

Specimen	N_{AISC}/N_{ue}	N_{BS5400}/N_{ue}	N_{EC4}/N_{ue}	N_{DBJ}/N_{ue}
Pa-6	0.90	0.93	0.93	0.97
Pb-6	0.88	0.91	0.91	0.95
Pc-6	0.82	0.85	0.85	0.89
Pd-6	0.78	0.80	0.81	0.85
Pe-6	0.77	0.78	0.79	0.83
Pa-10	0.84	0.86	0.86	0.95
Pb-10	0.81	0.82	0.82	0.94
Pc-10	0.85	0.86	0.87	1.01
Pd-10	0.88	0.89	0.90	1.08
Pe-10	0.90	0.92	0.92	1.13

Table 7
FE analysis results and comparison with test results

Specimen	$N_{u,FEA}$ (kN)	Δ_1 (%)	$N_{ut,FEA}/N_{u,FEA}$	$\sigma_{FEA,T}$ (MPa)	Δ_2 (%)
Pa-6-2	2801	-6.94	0.70	431	-
Pb-6-2	3063	-7.18	0.75	459	6.4
Pc-6-2	3398	-6.39	0.78	483	12.14
Pd-6-2	3779	-6.23	0.78	492	14.08
Pe-6-2	4106	-4.51	0.82	524	21.71
Pa-10-2	3769	-3.85	0.80	416	-
Pb-10-2	4135	-4.5	0.82	420	0.81
Pc-10-2	4344	0.09	0.83	423	1.56
Pd-10-2	4644	2.07	0.84	425	2.02
Pe-10-2	4945	6.92	0.85	431	3.54

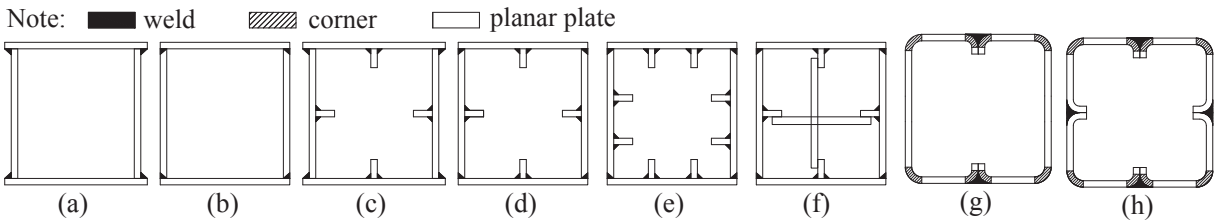

Fig. 1 Representative unstiffened and stiffened tubular sections of CFST columns from previous studies

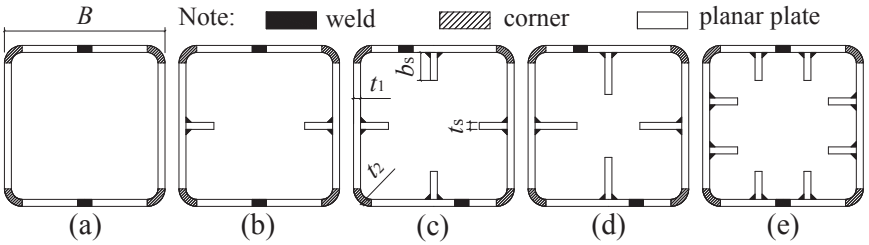

Fig. 2. Cold-formed steel tubular sections considered in this study

(a) (b) (c)

Fig. 3. Typical failure mode of the concrete specimens: (a) (b) cubic specimens (c) prismoid specimens

Fig. 4. Test setup of CFST-composite column specimen

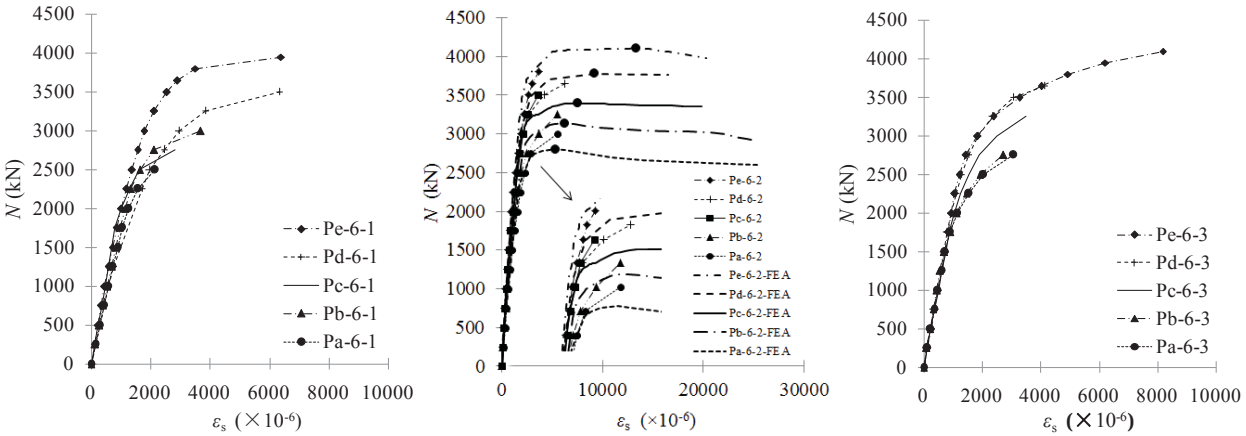

(a) Group 1 (b) Group 2 (c) Group 3

Fig.5 N versus ε_s curves of specimens with 6mm-thick wall tubes

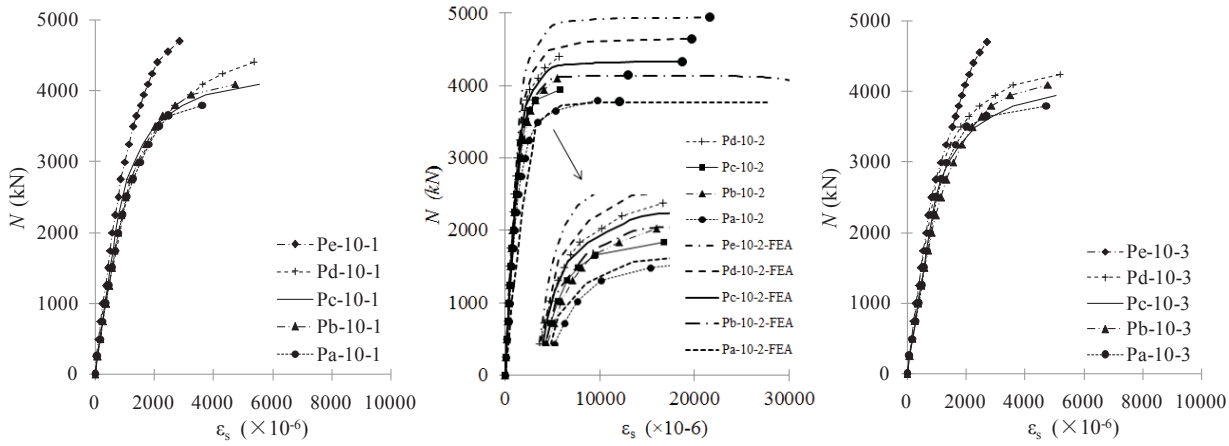

(a) Group 1 (b) Group 2 (c) Group 3

Fig.6 N versus ε_s curves of specimens with 10mm-thick wall tubes

(a) Pa-6-1 (b) Pb-6-2 (c) Pc-6-2 (d) Pd-6-2 (e) Pe-6-3 (f) Pa-10-1 (b) Pb-10-1 (c) Pc-10-2

Fig. 7 Typical failure mode for specimens

(a) Local buckling of unstiffened CFST section (b) Local buckling of stiffened CFST section

Fig. 8. Local buckling modes of test specimens in literatures

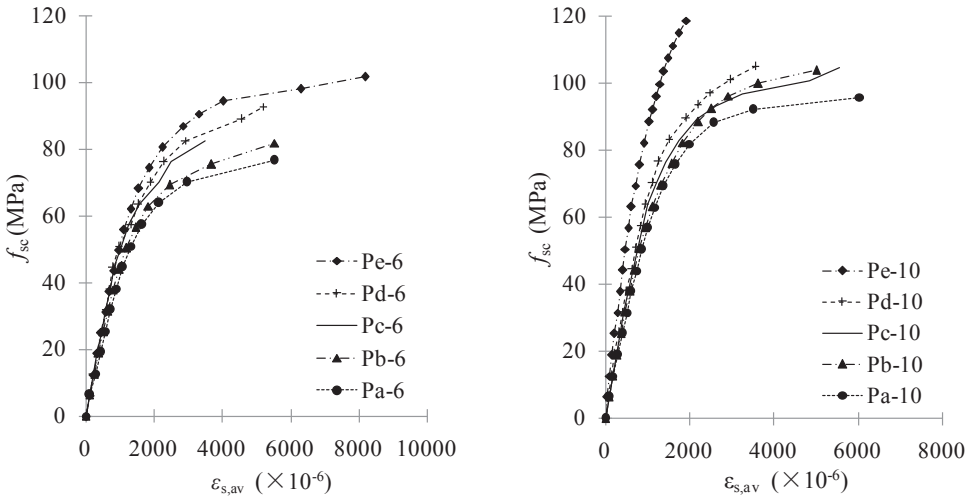

(a) Specimens with 6mm-thick tubes (b) Specimens with 10mm-thick tubes

Fig. 9. Average sectional stress (f_{sc}) versus average steel strain ($\varepsilon_{s,av}$) curves of specimens with same nominal sections

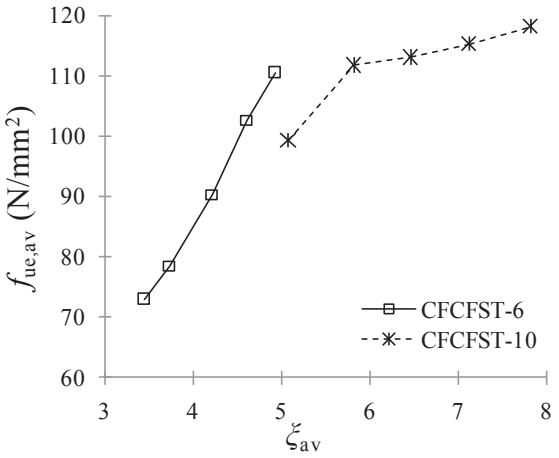

Fig. 10. $f_{ue,av}$ versus ξ_{av} curves

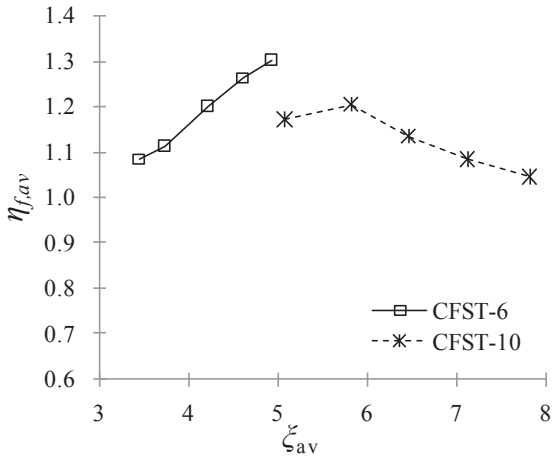

Fig. 11. $\eta_{f,av}$ versus ξ_{av} curves

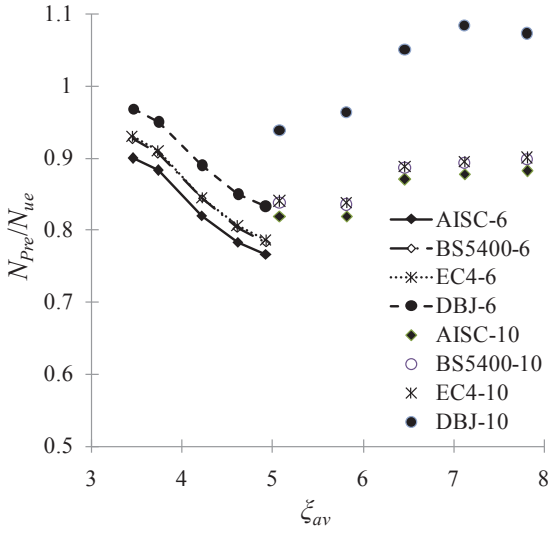

Fig. 12. Mean ratios of predicted capacity to test capacity (N_{pre}/N_{ue}) versus ξ_{av} curves

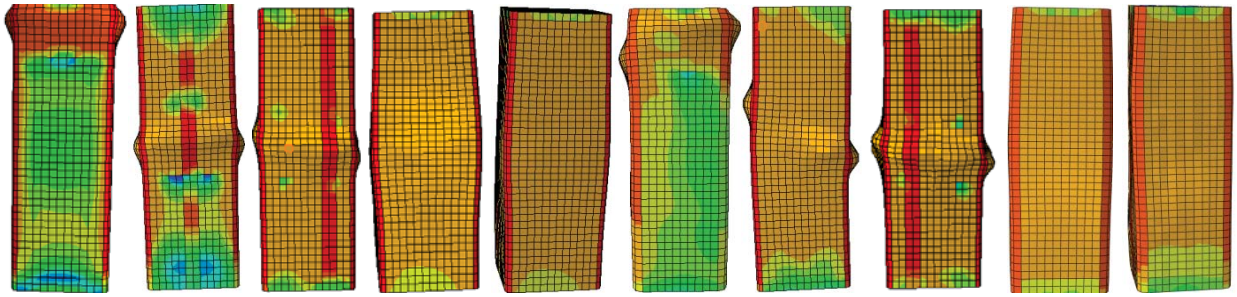

(a)Pa-6-2 (b)Pb-6-2 (c)Pc-6-2 (d)Pd-6-2 (e)Pe-6-2 (f)Pa-10-2 (g)Pb-10-2 (h)Pc-10-2 (i)Pd-10-2 (j)Pe-10-2

Fig. 13. Typical failure modes of specimens with tubular thickness of 6mm and 10mm (the colour scale relates to the plastic strain with the highest level occurring around local buckling regions)